Segmentation of Lung and its Lesions in Computer Tomographic Images

Sílvia Colella, Letícia Rittner
Medical Image Computing Lab (MICLab), School of Electrical and Computer Engineering
University of Campinas - UNICAMP, Campinas, Brazil
lrittner@dca.fee.unicamp.br

***Abstract*—The purpose of this work [1] is to propose two new automatic segmentation methods in computer tomographic (CT) images: one for the lungs and another one for their lesions. The lung segmentation method uses morphological filters and the max-tree - a data structure that represents an image through its connected components. Results show that the method presented a good performance when compared to the manual segmentation and it was able to not exclude lesions located in the borders in most of the images, which is challenging when the lesions are small and disconnected located in this region. The lung segmentation method obtained an average Dice of 98% for 630 slices (14 subjects). The lesion segmentation method uses the image with the segmented lungs as base to calculate the attributes of intensity, texture and distance transform to train a classifier that distinguishes between normal tissue and abnormal tissue (which contains lesions). The classifiers tested in this project were Random Forest and SVM. This method also presented good results as it turned out not being very sensible to parameters' choice and it obtained an average Dice of 62% for the slices with severe pathologies where the slices of 5 subjects were used for training and 1 for testing.**

I. Introduction

Human lungs can be affected by several respiratory diseases, like pneumonia and cancer. Some diseases, however, are not exclusively respiratory but can affect several organs including the lungs, known as interstitial lung diseases (ILDs), where we can have as examples the idiopathic pulmonary fibrosis and sarcoidosis. They are diseases that were put together due to their resemblance in presentation and radiological and clinical discoveries [1]. When these diseases reach the respiratory system, they can cause inflammation of the pulmonary tissue, which can be treated, or fibrosis, which is a permanent inflammation and, therefore, cannot be cured [2].

One of the ways to diagnose and follow up the evolution of the interstitial lung diseases is via diagnostic imaging, like computerized tomography (CT), an exam able to acquire a full view of the thorax in high resolution and in a single breath [3]. From the image analysis it is possible to evaluate the state of the lungs and, if the diagnosis is of a healthy lung, to avoid the need of a biopsy exam. The biopsy exam is a procedure that requires to withdraw a lung tissue sample to be examined in a lab, therefore it is considered an invading procedure. Figure 1 shows examples of CT images of the chest: healthy lung tissue, inflammation (ground glass) and fibrosis (honeycomb). The abnormal tissue is mostly located in the borders of the lungs as brighter spots, which confuses the gray levels between what belongs and what does not belong to the lungs.

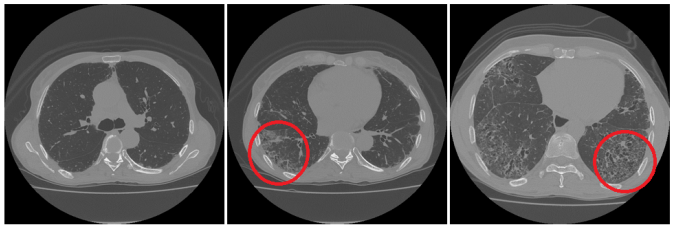

Fig. 1. CT images of the chest with healthy tissue (left), with inflammation (center) and with fibrosis (right).

In order to assist the analysis of the CT images, computer-aided diagnosis (CAD) systems are being developed to provide assistance to the specialist to make decisions about a diagnosis in a more accurate and faster way.

A pre-processing step usually done by CAD systems is the lung segmentation. Its goal is to distinguish the lung from the other structures in the image, like blood vessels and bones [4]. For subjects that do not present any disease (considered healthy), the automatic segmentation is a simple process. It becomes a challenge when the lungs present lesions located in the borders [3], just like the ILDs. As several diseases change the density of the lung tissue, they usually impact the intensity of the pixels (gray levels) in the CT images, therefore segmentation approaches that focus only in the intensity (usually chosen because they are efficient) do not work in most of these situations [3].

After the lung segmentation, the CAD systems start the process to distinguish between normal and abnormal tissue or between normal tissue and a wide variety of patterns, like emphysema, nodule, inflammation (ground glass) or fibrosis (honeycombing). It is an important process because, after the tissues are distinguished, it is possible to visualize and quantify how much of the lung tissue presents any pathology, which assists the radiologist with diagnosis and prognosis for a patient.

The great majority of works found in the literature about lung image processing is related to cancer due to its high mortality rate. Each lung nodule usually found in the CT images are a single connected component, which does not happen with the ILDs that present smaller and disconnected

[1]This work relates to a M.Sc. dissertation.

lesions. This feature is a challenge to the CAD systems, that must find the injured tissue and cannot mix the lesions with blood vessels from the inside of the lungs.

A. Objectives

This work has two main goals:

- to propose a new automated lung segmentation method in CT images based on max-tree and that does not exclude the lesions located in the borders. This approach does not require any manual interaction, pre-defined models or any anatomic starting point.
- to automatically segment lesions from the lung in the CT images by using machine learning algorithms. This approach has the automatic lung segmentation method as the only pre-processing step, so it does not require any manual interaction or starting point either.

B. Main contributions

The main contributions of this work are:

- completely automated methods, with no human interaction, no models and no starting point
- new methods concerning ILDs, as most of the work found in the state of the art focus on cancer nodules that present different features
- lesion segmentation and not only detection nor regions of interest (ROIs) classification

II. Proposed Method for Lung Segmentation based on Max-tree

1) Pre-processing: As the lungs are basically bags of air, they show up as dark regions in each slice of the CT image, so the first step of the process is to negate the image. When the image is negated, there is an inversion in the scale of gray levels, which can facilitate the search for the object of interest in medical images.

The next step is to apply the reconstructive filter with the purpose to smooth the gray levels in the image. The reconstructive filter alternates sequentially the close by reconstruction and open by reconstruction filters characterized by an structuring element during a defined number of iterations [5] (Fig. 3b).

2) Build and simplification of the max-tree: The lung segmentation approach is based on the max-tree, a structure with the purpose to represent all the connected components from all the possible thresholds of an image [6] (Fig. 2). Connected components are created when pixels connect to their neighbors, creating then a set of pixels depending on the chosen type of connectivity that could be 4, 6 or 8 [7].

The process to build the max-tree starts by the definition of the set of pixels from the background, which turns out to be a node for the tree. Next, the complementary set of pixels (that are not part of the background) create the connected components and become temporary child nodes (to be further analyzed). This process is repeated for each threshold [6].

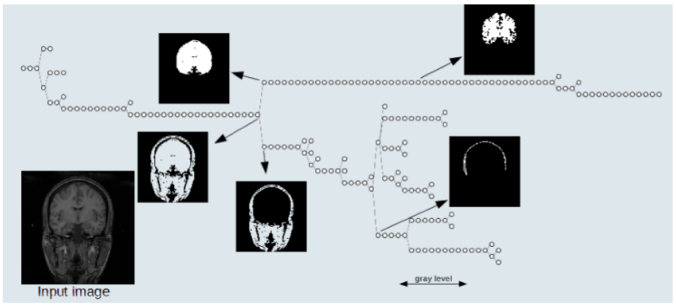

Fig. 2. Simplified illustration of a max-tree. The arrows point to the connected components that each node represents. (source: [8])

The max-tree represents an image by the hierarchical relationship of its connected components. Filtering the max-tree means to analyze each node using a established criteria and make a decision to remove or not the branch or the node [6]. By filtering the max-tree, the image it represents is also filtered, which facilitates processes like segmentation and smoothing. With the new simplified representation of the max-tree (now composed by less nodes), the filtered image can be rebuilt. After building the max-tree (with a 3x3 structuring element) the extinction filter was applied (a pruning strategy) [9], using the area as extinction value and defining the number of leaves to be kept as 6 (Fig. 3c). In the resulting max-tree the sixth node was chosen to represent each branch (a non-pruning strategy) [10] (Fig. 3d).

3) Lung Segmentation: The final step is the segmentation itself, which is the correct identification of the 2 nodes from the simplified max-tree that represent each one of the lungs. The chosen criteria were the area of the connected component and its rectangular format. Both criteria were defined by taking into consideration the shape of the objects of interest (Fig. 3e and 3f).

III. Proposed Method for Segmentation of Lung Lesions

1) Feature Extraction: After the lung segmentation, the next step was to search for features that could stress the fact that lesions show up as bright spots in the CT images and that they are located next to the lung borders. With that purpose on mind, the following features were chosen: intensity of the pixel, intensity of the pixel from the previous and posterior slices, the morphological gradient [11], the texture descriptor known as local binary pattern (LBP) [12], the Euclidean distance transform (EDT) [13] based on the original image and based on the image with the segmented lungs.

The intensity of the pixels from the current, previous and posterior slices were considered to assist the classifier to distinguish brighter dots (lesions) from darker dots (the remains of the lung). The morphological gradient was also chosen with this purpose: to emphasize the transitions in the gray levels and to separate brighter regions from darker ones.

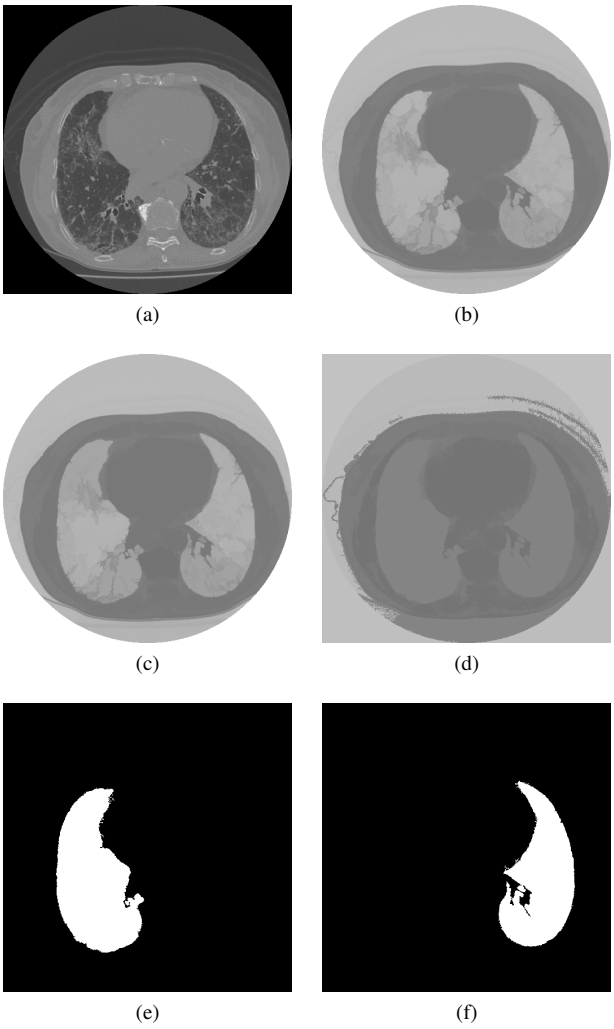

Fig. 3. Lung segmentation method applied to one slice: (a) original image, (b) negated image after applying the reconstructive filter (8 iterations), (c) resulting image after applying the extinction filter (n=6), (d) resulting image after choosing the sixth node to represent the branch, and finally choosing the correct nodes to represent (e) the right and (f) left lungs.

The LBP descriptor was chosen to distinguish the textures of the damaged tissue from the healthy tissue. And finally the EDT was used to stress the distance between the pixels and the borders of the image as the lesions are focused in the regions closer to the lung borders. This feature was used with the original image and the image with the segmented lungs, totalizing 7 features.

During the feature extraction process, only the features of the pixels belonging to the lungs are used (the pixels are compared with the resulting image of the lung segmentation process). The features were normalized between 0 and 1 to distribute the data equally so the values can be balanced and each feature has the same importance during the process.

2) Lesion Segmentation: The lesion segmentation process is performed by a pixel classifier, which is trained with labeled samples. After the training is completed, it classifies the unknown samples between two classes: lesion and non-lesion

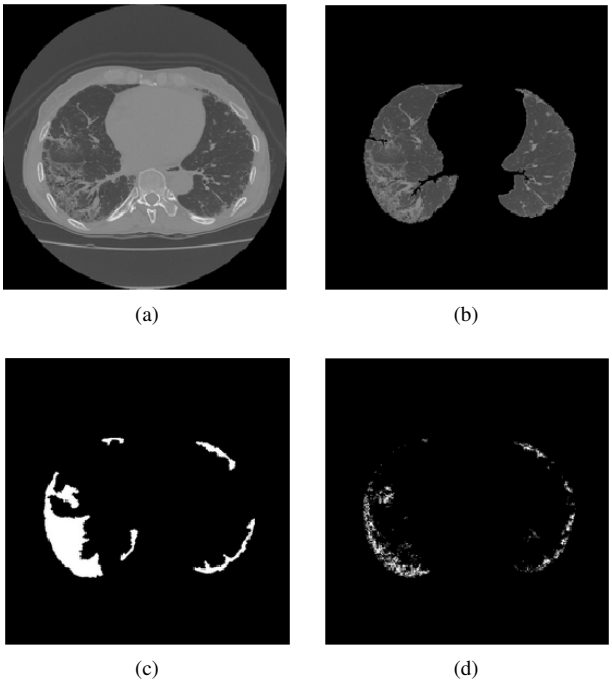

Fig. 4. Lesion segmentation method applied to one slice: (a) original image, (b) resulting image from lung segmentation process, (c) manually segmented lesions (ground-truth), (d) automatically segmented lesions (classifier's result).

(Fig. 4). The labeled samples were created under supervision from a specialist.

The classifiers considered for this process were *Random Forest*, which is based in decision trees to classify new objects [14], and *Support Vector Machines* (SVM), that during training it maps the inputs in a multidimensional space to find the best hyperplane that separates two classes. This hyperplane is then used to classify new inputs [15].

3) Post-processing: With the results obtained by the classifier, there is a requirement for a post-processing step to transform isolated pixel sets classified as lesions into one or more connected component. The Watershed Transform was then applied [16].

The reconstructive filter was applied to the original image and then the Sobel gradient was calculated in order to create the input image for the Watershed Transform (Fig. 5b). An area closing and an area opening filters were applied to the resulting image from the classifier so that could be used as internal marker: the area opening filter removed connected components with area less than 3 and the area closing filter removed connected components from the background with area less than 2. The external morphological gradient was used as external marker (Fig. 5c).

After applying the Watershed transform, the connected components with an area greater than 850 pixels were removed from the resulting image (Fig. 5e).

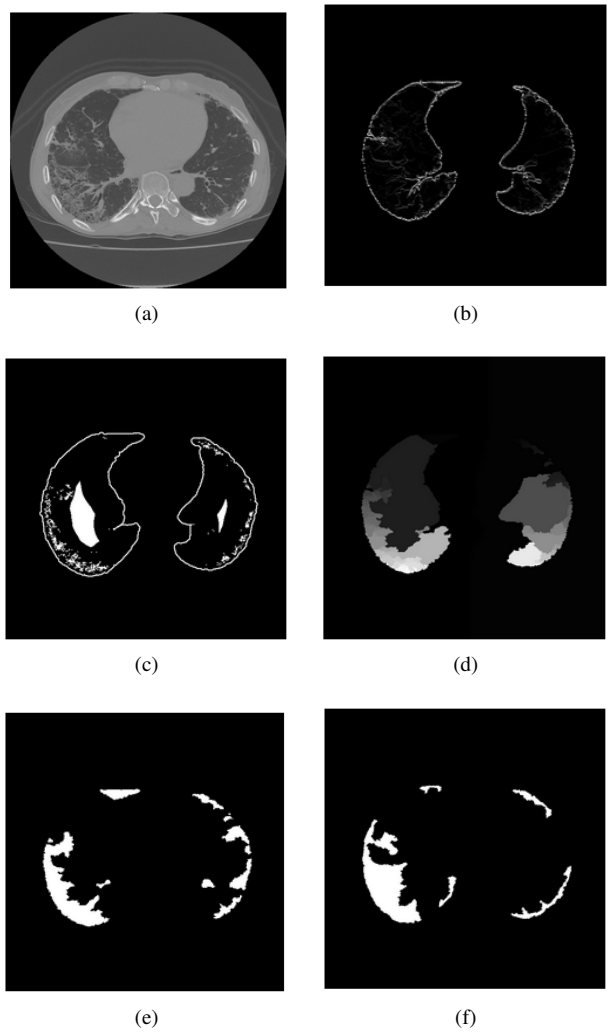

Fig. 5. Post-processing step applied to one slice: (a) original image, (b) input image, (c) internal and external markers, (d) output for the Watershed transform, (e) final image for the post-processing step, (f) manually segmented lesions (ground-truth).

IV. Results and Discussions

A. Experiments

The experiments were executed in the Adesssowiki environment, a collaborative platform for scientific studies and Python/C/C++ programming used for education and research of image processing algorithms [17]. All the code was developed in Python and several libraries were used: Numpy [18], the SDC Morphology Toolbox, the educational toolbox for max-tree called iamxt [17] and also the machine learning library in Python called scikit learn [19]. The authors also developed functions that were implemented during the project.

For the experiments CT images of the chest in the transverse plan were used from subjects with systemic sclerosis. The images are in the DICOM format and they were acquired from a Toshiba's Aquilion scanner, with 512x512 as resolution and slice thickness of 1.0mm. All the subjects were informed and signed a consent form approved by the Research Ethics Committee from FCM-UNICAMP (CEP 114069/2015; CAAE: 50830315.3.0000.5404).

From each acquired volume, only the slices located below the carina and above the liver were selected for the lung segmentation method, since the lesions are usually located in the inferior lobe of the right lung and in the central portions of both lungs [20]. The slices in this same location were also chosen for the lesion segmentation method, but only the ones that presented any lesion. Each slice was processed and segmented individually.

B. Results for Lung Segmentation Method

The results for each automatically segmented lung were compared with the manual segmentation provided by a specialist with the assistance from an interactive segmentation tool called Neuroline [21]. By lung segmentation, the specialist considered that the trachea and any other region outside of the lungs would not be included in the result.

In order to obtain a comparison of the results between subjects, 45 slices above the liver were separated for 14 different subjects. The evaluation method applied to this work was to calculate the rates for sensitivity, specificity and Dice coefficient (Tab. I and Fig. 6).

TABLE I
Performance rates for the automatic lung segmentation method for each subject in comparison with the manual segmentation, in the format (mean $\pm$ standard deviation)

ID	Sensitivity	Specificity	Dice
1	0.985 ± 0.010	0.995 ± 0.002	0.984 ± 0.005
2	0.989 ± 0.007	0.994 ± 0.002	0.984 ± 0.005
3	0.972 ± 0.015	0.992 ± 0.003	0.968 ± 0.011
4	0.980 ± 0.013	0.995 ± 0.002	0.970 ± 0.011
5	0.991 ± 0.013	0.993 ± 0.003	0.982 ± 0.010
6	0.987 ± 0.012	0.996 ± 0.003	0.978 ± 0.009
7	0.978 ± 0.013	0.996 ± 0.002	0.977 ± 0.009
8	0.983 ± 0.012	0.998 ± 0.003	0.987 ± 0.009
9	0.982 ± 0.012	0.996 ± 0.003	0.980 ± 0.009
10	0.995 ± 0.012	0.993 ± 0.003	0.986 ± 0.009
11	0.984 ± 0.012	0.996 ± 0.003	0.982 ± 0.009
12	0.983 ± 0.011	0.990 ± 0.003	0.977 ± 0.008
13	0.985 ± 0.011	0.998 ± 0.003	0.988 ± 0.009
14	0.982 ± 0.012	0.996 ± 0.003	0.984 ± 0.008

In both the table (Tab. I) and the boxplot (Fig. 6) it is possible to visualize that subject #3 is the one that most distances from the other subjects in numeric values. The images associated to this particular subject present lesions in the borders of the right lung and some of them even add external structures like the trachea (Fig. 7). In this case, the reconstructive filter used in the pre-processing step was not enough to ensure the correct segmentation. The same can be observed in some slices associated to subjects #4 and #12. In general, the method presented a good performance, as the minimum value for Dice coefficient was 0.968 and the maximum value was 0.988, totalizing 0.98 as average value for all the subjects with a standard deviation of 0.008.

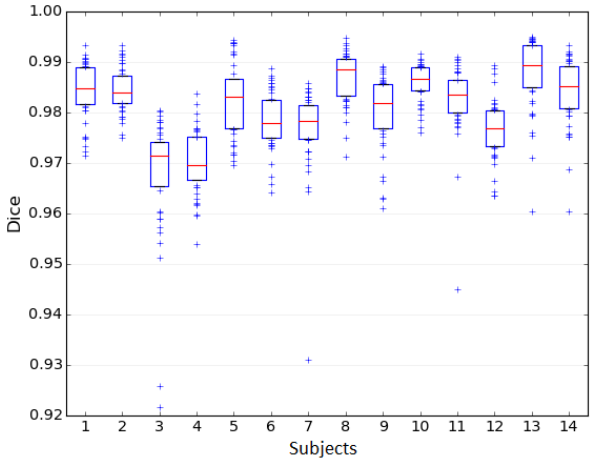

Fig. 6. Boxplot comparing the values obtained for Dice coefficient for all the 45 slices for each one of the analyzed subjects.

Fig. 7. Original slice from subject #3 (a), the result for the manual segmentation (b) and the result for the automatic segmentation method proposed (c), with an irregular border in the right lung.

Even though a direct comparison between the method presented here and related ones in the literature would only be possible if all of them used the same dataset, an overview (Tab. II) shows the results obtained by the proposed method and other approaches for lung segmentation in CT images that also used sensitivity, specificity and/or the Dice coefficient.

TABLE II
OVERVIEW INFORMATION ABOUT SOME OF THE MOST RECENT APPROACHES FOUND IN THE LITERATURE ABOUT LUNG SEGMENTATION IN CT IMAGES AND THE RATES ACHIEVED BY EACH ONE OF THEM (**SENSITIVITY**, **SPECIFICITY** AND **DICE**)

Paper	**S**	**E**	**D**
Proposed method	0.984 ± 0.005	0.995 ± 0.002	0.981 ± 0.008
Hua et al. (2011) [22]	0.986 ± 0.011	0.995 ± 0.003	N/A
Mansoor et al. (2014) [23]	0.96 and 0.97	0.92	0.95 and 0.96
Sluimer et al. (2004) [24]	0.92 ± 0.14	0.96 ± 0.02	N/A
Soliman et al. (2015) [25]	N/A	N/A	0.916
Sun et al. (2011) [26]	N/A	N/A	0.975 ± 0.006

C. Results for Lesion Segmentation Method

All the positive (with lesion) and negative (no lesion) samples of the slices that presented lesions were used during the process (15737308 processed pixels, with 1504250 positive samples). 328 slices from 5 subjects (from 52 to 85 slices per subject) were used for training. 32 slices from 1 subject was used for testing with unknown samples for the classifier, with half the slices with a large area of damaged tissue.

Regarding the evaluated classifiers used during this work, Random Forest got better results than linear SVM, specifically after adding weights to the classes and calibrating the classifier. Random Forest was able to correctly classify 1513299 samples, and SVM classified correctly 1307528 samples.

Even though SVM applied the lesion label correctly to more pixels than Random Forest, it also applied this same label incorrectly to a much bigger amount of pixels that should not receive it, showing that the SVM classifier could not distinguish the pixels as surely as the Random Forest one. Since this is a pixel classification, it is preferable a classifier that can well distinguish between pixels because even if it returns a smaller amount of pixels with lesion, they are well positioned and can be used as seeds for the post-processing step. With that in mind, the Watershed transform was applied, where the results from the classifier were used as internal markers after applying the area opening and area closing filters.

The results from the automatic lesion segmentation method were also compared with the manual segmentation provided by a specialist using the Neuroline tool [21]. For all the 32 slices used for testing, the mean values calculated for sensitivity, specificity and Dice coefficient were 0.566 ± 0.14, 0.987 ± 0.007 and 0.474 ± 0.28 respectively. From the 32 slices, half of them is located closer to the liver and presented a large area of damaged tissue (due to the fact that this location has a bigger probability to find these lesions [20]) and for these slices the mean values for sensitivity, specificity and Dice coefficient were 0.629 ± 0.118, 0.992 ± 0.003 and 0.632 ± 0.057 respectively. Fig. 8 shows the difference found for the Dice coefficient before and after the post-processing step for all the 32 slices on the left and the same difference for the 16 slices with a large area of damaged tissue on the right.

Regarding the state of the art, the work from Sluimer et al. (2003) [27] is the one closest to this proposed work because it also had the goal to distinguish healthy tissue from damaged tissue. However there is a fundamental difference: the method developed by Sluimer et al. only classifies circular ROIs that were manually selected while the method proposed here classifies pixel per pixel, identifying them as part of a lesion or not, which is a more difficult job. That explains the difference in the results obtained by both methods, besides the fact that they were calculated for different datasets: the value obtained for the area under the ROC curve was 0.775 ± 0.069 for the pixel classification proposed here and 0.862 for the ROI classification.

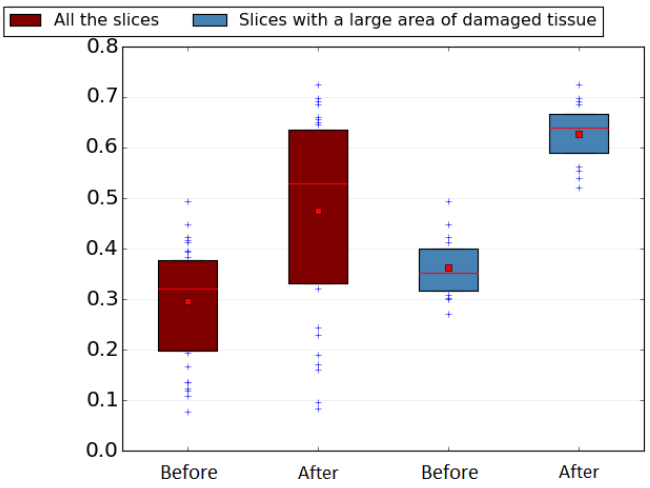

Fig. 8. Boxplot comparing the values for the Dice coefficient before and after the post-processing step.

V. Conclusion

The main contributions for this work were the proposal of two new segmentation methods focused on ILDs: one for the lungs and one for their lesions, both completely automatic. The lung segmentation method was developed to ensure a correct segmentation even when the lungs present lesions in the borders. The second method, unlike most approaches found in the literature, not only detects the lesions but it also segments the damaged region of the lung tissue.

Several parameters were varied to test which ones would have better results for the testing set for the two segmentation methods. Both methods showed to not be very sensitive to parameters, which also shows the good results obtained by the proposed methods.

The results obtained by the lung segmentation method were presented at the XXV Brazilian Congress on Biomedical Engineering (CBEB) with the title *Método automático de segmentação dos pulmões em imagens de CT baseado na max-tree* and was published in the proceedings of the event [28].

References

[1] B. G. Baldi and C. A. Pereira, "Diretrizes de doenas pulmonares intersticiais da sociedade brasileira de pneumologia e tisiologia," *Jornal Brasileiro de Pneumologia*, vol. 38, pp. S1–S133, 2012.

[2] J. A. B. Martinez, "Doenas intersticiais pulmonares," *Revista Medicina da USP*, vol. 31, pp. 247–256, 1998.

[3] I. Sluimer, A. Schilham, M. Prokop, and B. van Ginneken, "Computer analysis of computed tomography scans of the lung: a survey," *IEEE Transactions on Medical Imaging*, April 2006.

[4] A. Mansoor, U. Bagci, B. Foster, Z. Xu, G. Z. Papadakis, L. R. Folio, J. K. Udupa, and D. J. Mollura, "Segmentation and image analysis of abnormal lungs at ct: Current approaches, challenges, and future trends," *RadioGraphics*, vol. 35, no. 4, pp. 1056–1076, 2015, pMID: 26172351.

[5] L. Vincent, "Morphological grayscale reconstruction in image analysis: applications and efficient algorithms," *IEEE Transactions on Image Processing*, vol. 2, no. 2, pp. 176–201, Apr 1993.

[6] P. Salembier, A. Oliveras, and L. Garrido, "Anti-extensive connected operators for image and sequence processing," *IEEE Transactions on Image Processing*, 1998.

[7] P. Salembier and J. Serra, "Flat zones filtering, connected operators, and filters by reconstruction," *IEEE Transactions on Image Processing*, vol. 4, no. 8, pp. 1153–1160, Aug 1995.

[8] R. Souza, L. Tavares, L. Rittner, and R. Lotufo, "An overview of max-tree principles, algorithms and applications," in *Proceedings...*, Conference on Graphics, Patterns and Images, 29. (SIBGRAPI). Porto Alegre: Sociedade Brasileira de Computação, 2016.

[9] C. Vachier and F. Meyer, "Extinction value: a new measurement of persistence," *IEEE Workshop of Nonlinear Signal and Image Processing*, 1995.

[10] L. A. Tavares, R. M. Souza, L. Rittner, R. C. Machado, and R. A. Lotufo, "Interactive max-tree visualization tool for image processing and analysis," in *2015 International Conference on Image Processing Theory, Tools and Applications (IPTA)*, Nov 2015, pp. 119–124.

[11] R. Gonzalez and R. Woods, *Digital Image Processing*. Pearson Education, 2009.

[12] M. Heikkil, M. Pietikinen, and C. Schmid, "Description of interest regions with local binary patterns," *Pattern Recognition*, vol. 42, no. 3, pp. 425 – 436, 2009.

[13] R. Fabbri, L. D. F. Costa, J. C. Torelli, and O. M. Bruno, "2d euclidean distance transform algorithms: A comparative survey," *ACM Comput. Surv.*, vol. 40, no. 1, pp. 2:1–2:44, Feb. 2008.

[14] T. K. Ho, "Random decision forests," in *Proceedings of the Third International Conference on Document Analysis and Recognition (Volume 1) - Volume 1*, ser. ICDAR '95. Washington, DC, USA: IEEE Computer Society, 1995, pp. 278–.

[15] C. Cortes and V. Vapnik, "Support-vector networks," *Mach. Learn.*, vol. 20, no. 3, pp. 273–297, Sep. 1995.

[16] J. B. Roerdink and A. Meijster, "The watershed transform: Definitions, algorithms and parallelization strategies," *Fundam. Inform.*, vol. 41, no. 1-2, pp. 187–228, 2000.

[17] R. Lotufo, R. Machado, A. Korbes, and R. Ramos, "Adessowiki: on-line collaborative scientific programming platform," *Proceedings of the 2009 International Symposium on Wikis, 2009, Orlando, Florida, USA*, 2009.

[18] S. Walt, S. Colbert, and G. Varoquaux, "The NumPy Array: A Structure for Efficient Numerical Computation," *Computing in Science & Engineering*, vol. 13, no. 2, pp. 22–30, 2011.

[19] F. Pedregosa, G. Varoquaux, A. Gramfort, V. Michel, B. Thirion, O. Grisel, M. Blondel, P. Prettenhofer, R. Weiss, V. Dubourg, J. Vanderplas, A. Passos, D. Cournapeau, M. Brucher, M. Perrot, and E. Duchesnay, "Scikit-learn: Machine learning in Python," *Journal of Machine Learning Research*, vol. 12, pp. 2825–2830, 2011.

[20] E. L. Gasparetto, R. Pimenta, C. Inoue, S. E. Ono, and D. L. Escuissato, "Esclerose sistêmica progressiva: aspectos na tomografia computadorizada de alta resolućão," *Radiologia Brasileira*, vol. 38, pp. 329 – 332, 09 2005.

[21] A. Carnevalle, J. Rondina, E. Kobayashi, and F. Cendes, "Validation of a semi-automated system for mri-based hippocampal volumetry in patients with temporal lobe epilepsy," *J Epilepsy Clin Neurophysiol*, 2003.

[22] P. Hua, Q. Song, M. Sonka, E. A. Hoffman, and J. M. Reinhardt, "Segmentation of pathological and diseased lung tissue in ct images using a graph-search algorithm," in *2011 IEEE International Symposium on Biomedical Imaging: From Nano to Macro*, March 2011.

[23] A. Mansoor, U. Bagci, Z. Xu, B. Foster, K. N. Olivier, J. M. Elinoff, A. F. Suffredini, J. K. Udupa, and D. J. Mollura, "A generic approach to pathological lung segmentation," *IEEE Transactions on Medical Imaging*, vol. 33, no. 12, pp. 2293–2310, Dec 2014.

[24] I. C. Sluimer, M. Niemeijer, and B. van Ginneken, "Lung field segmentation from thin-slice ct scans in presence of severe pathology," *Proc. SPIE*, vol. 5370, pp. 1447–1455, 2004.

[25] A. Soliman, A. Elnakib, F. Khalifa, M. A. El-Ghar, and A. El-Baz, "Segmentationof pathological lungs from ct chest images," in *Image Processing (ICIP), 2015 IEEE International Conference on*, Sept 2015, pp. 3655–3659.

[26] S. Sun, C. Bauer, and R. Beichel, "Automated 3-d segmentation of lungs with lung cancer in ct data using a novel robust active shape model approach," *IEEE Transactions on Medical Imaging*, Feb 2012.

[27] I. C. Sluimer, P. F. van Waes, M. A. Viergever, and B. van Ginneken, "Computer-aided diagnosis in high resolution ct of the lungs," *Medical Physics*, vol. 30, no. 12, pp. 3081–3090, 2003.

[28] S. Colella, S. Appenzeller, S. Dertkigil, and L. Rittner, "Método automático de segmentação dos pulmões em imagens de ct baseado na max-tree," in *Proceedings of XXV Congresso Brasileiro de Engenharia Biomédica*, 2016.